

# Bulky glycocalyx drives cancer invasiveness by modulating substrate-specific adhesion

Amlan Barai  <sup>a,1</sup>, Niyati Piplani  <sup>a</sup>, Sumon Kumar Saha  <sup>a</sup>, Sarbajeet Dutta <sup>a</sup>, V. Gomathi  <sup>b</sup>, Mayank M. Ghogale  <sup>a</sup>, Sushil Kumar  <sup>a</sup>, Madhura Kulkarni  <sup>b</sup> and Shamik Sen  <sup>a,\*</sup>

<sup>a</sup>Department of Biosciences and Bioengineering, IIT Bombay, Mumbai 400076, India

<sup>b</sup>Center for Translational Cancer Research, IISER Pune and PCCM Pune, Pune 411008, India

\*To whom correspondence should be addressed: Email: [shamiks@iitb.ac.in](mailto:shamiks@iitb.ac.in)

<sup>1</sup>Present address: CNRS, Université Paris Cité, Institut Jacques Monod, Paris 75013, France.

Edited By JoAnn Trejo

## Abstract

The majority of the eukaryotic cell surface is decorated with a layer of membrane-attached polysaccharides and glycoproteins collectively referred to as the glycocalyx. While the formation of a bulky glycocalyx has been associated with the cancer progression, the mechanisms by which the glycocalyx regulates cancer invasiveness are incompletely understood. We address this question by first documenting subtype-specific expression of the major glycocalyx glycoprotein Mucin-1 (MUC1) in breast cancer patient samples and breast cancer cell lines. Strikingly, glycocalyx disruption led to inhibition of 2D motility, loss of 3D invasion, and reduction of clonal scattering in breast cancer cells at the population level. Tracking of 2D cell motility and 3D invasiveness of MUC1-based sorted subpopulations revealed the fastest motility and invasiveness in intermediate MUC1-expressing cells, with glycocalyx disruption abolishing these effects. While differential sensitivity in 2D motility is attributed to a nonmonotonic dependence of focal adhesion size on MUC1 levels, higher MUC1 levels enhance 3D invasiveness via increased traction generation. In contrast to inducing cell rounding on collagen-coated substrates, high MUC1 level promotes cell adhesion and confers resistance to shear flow on substrates coated with the endothelial surface protein E-selectin. Collectively, our findings illustrate how MUC1 drives cancer invasiveness by differentially regulating cell–substrate adhesion in a substrate-dependent manner.

## Significance Statement

The glycocalyx is a layer of polysaccharides and glycoproteins that cover the surface of most eukaryotic cells. We studied how malignancy-associated bulky glycocalyx affects cancer invasion stages. Mucin-1 (MUC1), a major bulky glycocalyx, was examined in cancer patient samples and cell lines. We found glycocalyx disruption inhibits movement in 2D and invasion in 3D, and prevents clonal scattering. Intermediate MUC1-expressing cells had the highest motility and invasiveness, and glycocalyx disruption eliminated these effects. Higher MUC1 levels increased traction generation, which enhanced 3D invasiveness. High MUC1 levels promoted cell adhesion and resistance to shear flow on selectin-coated substrates, but induced cell rounding on collagen-coated substrates. Our findings suggest that MUC1 drives cancer invasiveness by differentially regulating cell–substrate adhesion in a substrate-specific manner.

## Introduction

The cell interface is critical in terms of maintaining cell–substrate interactions. The cell senses its surroundings and responds accordingly using different receptors on the cell surface, of which perhaps the most important are a group of molecules that regulate cell–substrate adhesions. Integrins—which mediate cell–matrix adhesions—form cellular mechanosensory components that can regulate cytoskeletal architecture and control cellular dynamic properties, including cell shape change and cell migration (1–4). Mammalian cells are often coated with a layer of sugars mainly of glycoproteins and glycolipids in origin, which are

collectively referred to as the glycocalyx (5). The glycocalyx layer forms a coat around the cell; hence, most of the surface signal receptors, including integrins and cadherins, are buried in the glycan crowd. Therefore, changes in the glycan layer are expected to significantly impact various surface signaling pathways. In addition, since glycocalyx is the outermost layer and is in direct physical contact with the cell surroundings, the biophysical properties of the glycan layer should greatly impact cell–substrate interactions, and consequently, cell–substrate adhesions.

The glycocalyx layer shows a remarkable change in its composition and organization during development and disease like

**Competing Interest:** The authors declare no competing interests.

**Received:** November 14, 2023. **Accepted:** July 30, 2024

© The Author(s) 2024. Published by Oxford University Press on behalf of National Academy of Sciences. This is an Open Access article distributed under the terms of the Creative Commons Attribution-NonCommercial-NoDerivs licence (<https://creativecommons.org/licenses/by-nc-nd/4.0/>), which permits non-commercial reproduction and distribution of the work, in any medium, provided the original work is not altered or transformed in any way, and that the work is properly cited. For commercial re-use, please contact [reprints@oup.com](mailto:reprints@oup.com) for reprints and translation rights for reprints. All other permissions can be obtained through our RightsLink service via the Permissions link on the article page on our site—for further information please contact [journals.permissions@oup.com](mailto:journals.permissions@oup.com).



cancer (6–10). Recent studies have demonstrated that malignant cancer cells often overexpress a group of transmembrane glycoproteins called mucins that make up most of the cell surface glycan structure commonly referred to as the bulky glycocalyx. The mucin family includes several transmembrane proteins characterized by extensive glycosylation of proline, threonine, and serine-rich domains (PTS domain). Mucin-1 (hereafter referred to as MUC1) has been more extensively studied among other mucins and its overexpression has been documented in multiple cancers, including breast cancer (10–13). Instead of exhibiting an apical localization profile, MUC1 localizes all over the cell surface in cancer cells. These alterations in expression and localization may trigger the loss of adhesions and increased invasiveness. Consistent with this, MUC1 transfection in human pancreatic and gastric cells led to decreased adhesion to type I collagen, type IV collagen, fibronectin, and laminin, but increased motility and *in vitro* invasiveness (14, 15). In contrast, the inhibition of MUC1 in human pancreatic cancer cells led to slower proliferation, increased cell-matrix adhesion, and reduced lymph node metastasis (16–18).

While these studies are indicative of an inverse correlation between MUC1 expression and cell-matrix adhesions, in a seminal study, Paszek et al. (19–21) demonstrated that a bulky glycocalyx formed by overexpressing the extracellular domain of MUC1 can drive tumor progression through the formation of integrin-based adhesions and integrin-based signaling. The bulkiness of MUC1 can create steric hindrance and induce integrin funneling into preexisting adhesions, thereby effectively increasing the size of adhesions (14–16). Recent studies have also demonstrated significant contributions of the surface glycocalyx in cell membrane shape regulation and membrane protrusion formation (22, 23). Collectively, these studies suggest that MUC1 regulates invasiveness by modulating cell-matrix adhesion. However, how such alterations impact different stages of invasion (e.g. invasion through the stroma or in circulation) remains unclear.

This study investigates glycocalyx alterations associated with cancer, and their biophysical role in regulating cell–substrate adhesions and cancer invasiveness. We found altered glycocalyx expression and localization differentially regulate the cell–substrate adhesion in a substrate-dependent manner. With increasing mucin levels, cell initially transforms from epithelial to mesenchymal state, and further increases help them to transform to a circulating tumor cell-like stage.

## Results

### MUC1 expression and/or glycosylation are elevated in breast cancer

Aberrant glycosylation and up-regulation of bulky glycocalyx have already been reported in various cancer cells, including pancreatic cancer, lung cancer, ovarian cancer, bladder cancer, and prostate cancer (6, 13, 14, 24, 25). Copy number alterations (CNAs) encompass gene amplifications, gains, deep, or shallow deletions play a crucial role in cancer development and progression. We performed CNA analysis of mucin genes to identify genomic alterations in breast cancer patient samples. Oncoprint represented the distribution of CNAs in mucin (Fig. S1). Noticeably, the MUC1 gene had the highest probability of genomic amplifications (21% in METABRIC and 12% in Firehose Legacy) among mucins, suggesting a potential oncogenic role of MUC1. Our immunohistochemical staining revealed that ER+ and HER2+ breast tumors have high mucin expression; especially, the aggressive HER2+ breast cancer shows significantly more MUC1-positive fraction compared with

triple-negative breast cancer (TNBC; Fig. 1A and B). However, MUC1 expression was not significantly increased in ER+ tumor when compared with ER- tumor (Fig. 1C).

Next, we assayed MUC1 expression in breast cancer cell lines. In comparison with nonmalignant MCF10A cells, MUC1 expression was up-regulated in both MCF7 and MDA-MB-231 (hereafter referred to as MDA231) cells (Fig. 1D). Consistent with transcript profiles, Fluorescence-activated cell sorting (FACS) analysis revealed mostly MUC1-negative (MUC1-Neg) cells in MCF10A cells (Fig. 1E). Interestingly, considerable heterogeneity in MUC1 expression was observed in MCF7 cells with the presence of low MUC1 (MUC1-Low)- and high MUC1 (MUC1-High)-expressing cells, as well as a small subpopulation of MUC1-Neg cells. While FACS staining revealed the presence of MUC1-Neg and MUC1-Low subpopulations in MDA231 cells, a substantial increase in the proportion of MUC1-positive cells upon neuraminidase (NMase) treatment suggests that increased MUC1 glycosylation in MDA231 cells is restrictive for antibody to stain MUC1, as reported elsewhere (26). Confocal imaging further confirmed the presence of MUC1 on the cell surface of MCF7 and MDA231 cells and its absence in MCF10A cells. To test overall glycocalyx levels in these three cell types, we stained cells using wheat germ agglutinin (WGA), a lectin that largely stains sialic acid and associated sugars. The staining revealed that both MCF7 and MDA231 have an overall more glycosylated surface compared with MCF10A (Fig. 1F). Together, these results reveal increased MUC1 levels and its glycosylation in breast cancer cells compared with nontransformed cells.

### Enzymatic deglycosylation of cell surface glycocalyx reduces cancer invasiveness

The sugar residues on the glycoprotein provide stability and hence, the removal of sugar leads the glycan layer to collapse. NMase from *Clostridium perfringens* partially deglycosylates the glycan layer thereby reducing the surface glycan layer density (Fig. 2A and B). The NMase treatment that removes existing glycocalyx layer was combined with Tunicamycin treatment that inhibits de novo glycosylation (17, 27). Enzyme treatment up to 36 h showed no significant impact on cell viability as checked via MTT (3-(4, 5-dimethylthiazolyl-2)-2, 5-diphenyltetrazolium bromide) assay; hence, all the experiments were performed before 36 h time point (Fig. S2).

To test the role of glycocalyx on cell invasiveness, we checked cell migration using live-cell migration setup in MCF7 and MDA231 cells (Fig. 2C). Deglycosylation with NMase treatment led to a significant reduction in 2D cell motility in both MCF7 and MDA231 cells. To test whether a similar phenomenon is observed in the 3D scenario, we encapsulated cells in collagen hydrogels that more closely mimic the *in vivo* stroma and checked cell invasiveness after glycan disruption. In 3D also, the cells showed a similar response where the cell invasiveness dropped significantly upon NMase treatment (Fig. 2D). In comparison, non-malignant MCF10A cells did not show any significant change upon NMase treatment (Fig. S3). In line with these observations, enzymatic deglycosylation also led to decreased spheroid invasion in MCF7 and MDA231 cells (Fig. 2E and F). To test whether these effects are specific to NMase, we have also performed 3D invasion experiments using MCF10A, MCF7, and MDA231 cells in the presence of StcE mucinase. Similar to NMase treatment, mucinase treatment led to reduced invasiveness (Fig. S4A and B). This independently confirms the role of endogenous MUC1 in regulating invasiveness. Together, these observations suggest that glycan removal negatively impacts migration and invasion of cells, while noncancerous cells remain unimpacted.

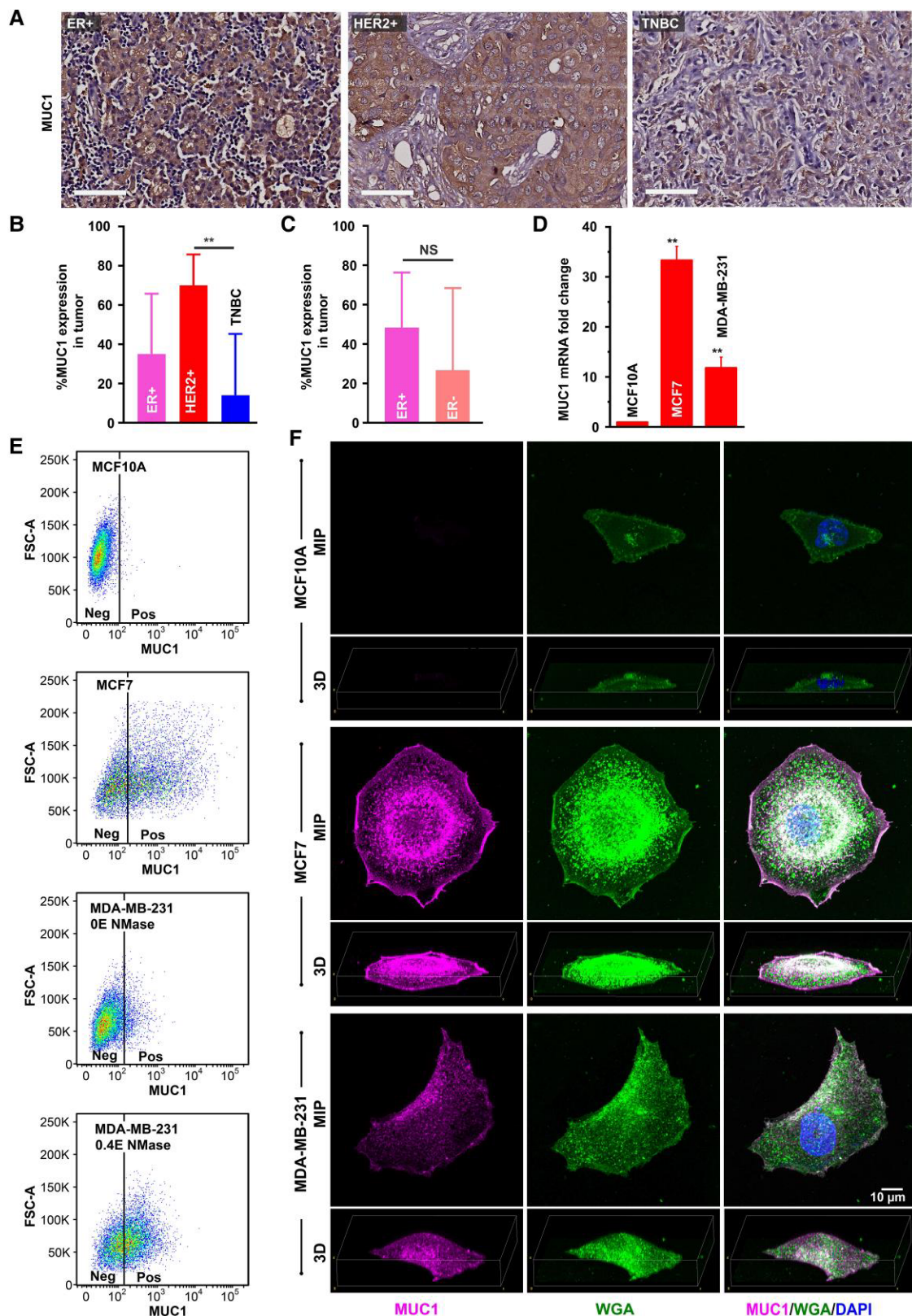


**Fig. 1.** Cell surface bulky glyocalyx is up-regulated in cancer. **A)** Representative images of MUC1 immunohistochemical staining in ER+, HER2+, and TNBC tissue. Scale bar, 50  $\mu$ m. Quantification of MUC1 expression from immunohistochemical staining from ER+, HER2+, and TNBC staining ( $n = 5$  in each case) in (B) and ER+ ( $n = 6$ ) and ER- ( $n = 9$ ) samples in (C) (\*\* $P < 0.005$ , ns, nonsignificant  $P > 0.05$ , data are presented as mean  $\pm$  SD). **D)** Analysis of MUC1 mRNA transcripts using real-time PCR. Total RNA harvested from 24 h culture of MCF10A, MCF7, and MDA231 cells were subjected to quantitative real-time PCR analysis. The graph shows mRNA fold change compared with MCF10A ( $n \geq 3$ , \*\* $P < 0.001$ ; values indicate mean  $\pm$  SEM). **E)** FACS analysis of cell surface MUC1 expression in MCF10A, MCF7, and MDA231 cell population. **F)** Confocal microscopy images showing surface glycan distribution in MCF7 and MDA231 cells. Unpermeabilized cells were stained with MUC1 antibody and FITC-WGA (Lectin) and then glyocalyx was visualized from maximum intensity projection (MIP) and reconstituted 3D image. F-actin was stained with phalloidin and nucleus was stained with DAPI. Scale bar, 10  $\mu$ m.

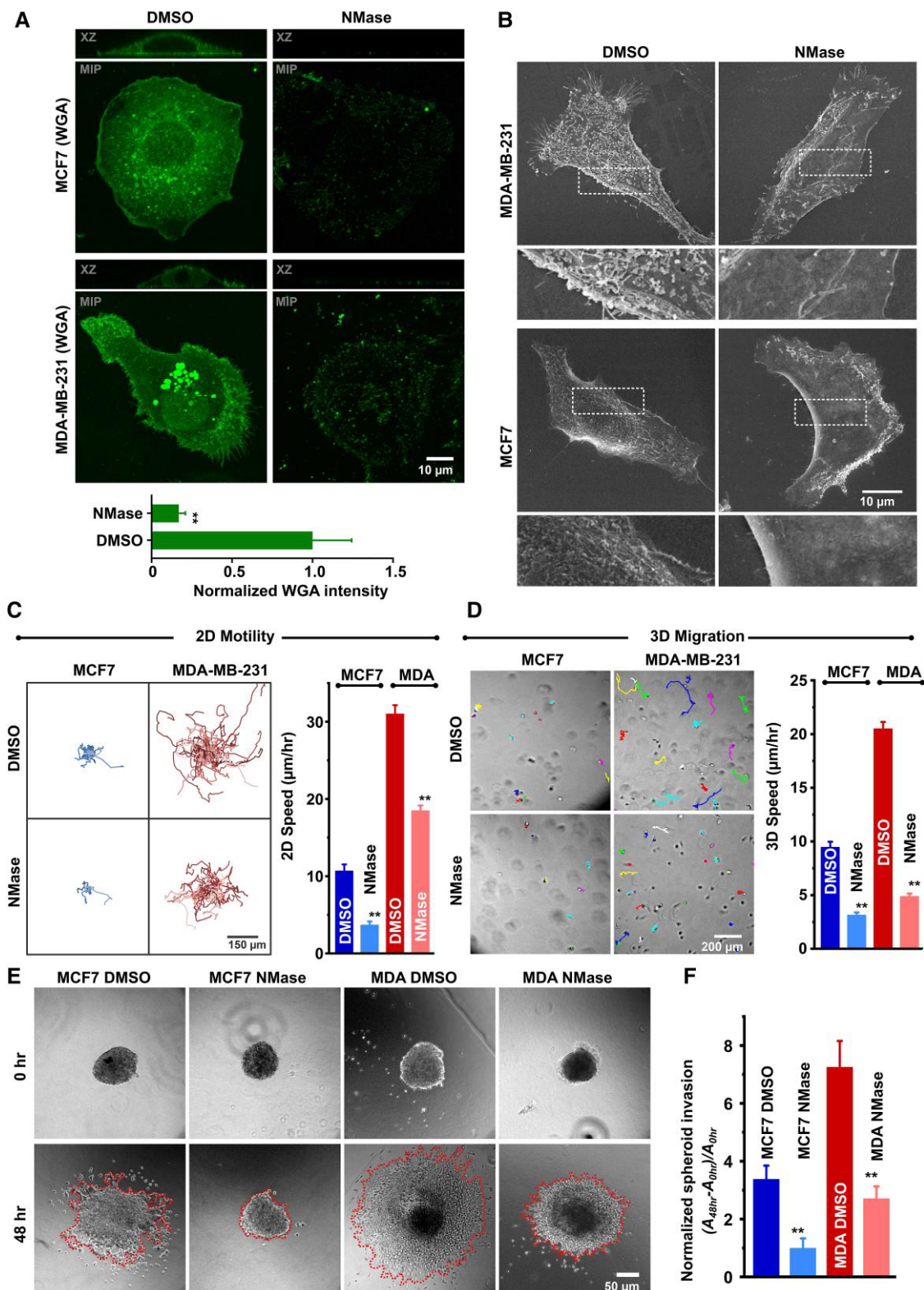


**Fig. 2.** Enzymatic deglycosylation of cancer cell surface glycocalyx reduces invasiveness. **A)** Confocal microscopy images showing MIP and XZ projection of FITC-WGA-stained MCF7 and MDA231 cell after 3 h Dimethyl sulfoxide (DMSO) or 0.4 U/mL NMase treatment. The bottom panel shows WGA intensity quantification from obtained confocal images ( $n = 2, 10$  confocal z-stack per conditions,  $^{**}P < 0.005$ , data presented as mean  $\pm$  SEM). **B)** FEG-SEM images showing membrane microarchitecture of untreated (DMSO) and NMase-treated (0.4 U/mL NMase) MCF7 and MDA231 cells. **C)** Left: Representative trajectories of MCF7 and MDA231 cells migrating on collagen-coated cell culture plate in the presence of 0.4 U/mL NMase and 20  $\mu$ g/mL Tunicamycin (NMase) or vehicle (DMSO). Right: Quantification of 2D speed ( $n = 3$ , per condition  $> 70$  cells,  $^{**}P < 0.005$ , data are presented as mean  $\pm$  SEM). **D)** Right: Representative microscopic frames showing cells encapsulated in 1.5 mg/mL 3D collagen gel with movement trajectories of MCF7 and MDA231 cells with NMase or DMSO treatment. Left: Quantification of 3D speed ( $n = 3$ , per condition  $> 110$  cells,  $^{**}P < 0.005$ , data are presented as mean  $\pm$  SEM). **E)** Representative phase-contrast images showing spheroid invasion assay in 3D collagen. Spheroids prepared from MCF7 and MDA231 cells were embedded in 3D collagen layer in the presence of NMase or DMSO treatment and images were taken at 0 and 48 h time points. **F)** Quantification of spheroid invasion ( $n = 3$ , 5–10 spheroids per condition,  $^{**}P < 0.005$ , data are presented as mean  $\pm$  SEM).

## Intermediate level of glycocalyx promotes invasiveness by regulating cell-matrix adhesions

Thus far, we have established that the presence of a glycocalyx increases cancer cell migration. To test whether different levels of surface glycocalyx differentially regulate cell migration, we have FACS-sorted MCF7 cells, which exhibit a wide range of glycan distribution, into three subpopulations based on MUC1 expression (Fig. 3A). Lectin staining of sorted MUC1-Neg cells, MUC1-Low-expressing cells, and MUC1-High-expressing cells revealed a close correlation between overall glycocalyx density and MUC1 expression (Fig. 3B). In comparison with the flattened morphologies of MUC1-Neg cells, MUC1-Low and MUC1-High were comparably rounded, with NMase treatment of MUC1-High cells leading to flattening similar to that of MUC1-Neg cells (Fig. 3C).

Motility experiments on collagen-coated dishes revealed that MUC1-positive cells (i.e. MUC1-Low and MUC1-High) migrate faster than MUC1-Neg cells. Surprisingly, MUC1-Low cells were found to migrate several times faster than MUC1-High cells (Fig. 3D and E). This differential migratory phenotype can be attributed to the surface glycocalyx density as enzymatic deglycosylation reduced migration speeds to levels comparable with that of MUC1-Neg cells across all conditions (Fig. 3D and E).

When cells were seeded sparsely and allowed to form microcolonies, MUC1-Neg cells were found to form compact epithelial-like colonies with low intercellular distance, while MUC1-positive cells formed sparse colonies with greater intercellular distance resembling a more mesenchymal phenotype (Fig. 3F and G). To determine whether there is a connection between epithelial to mesenchymal transition (EMT) signatures and MUC1 expression, we used scGSEA to evaluate EMT pathway activity and compared it with MUC1 expression in primary tumor cells. However, no correlation between MUC1 expression and EMT signature scores was observed ( $R^2 < 0.0001$ , Fig. S5A). Furthermore, profiling of EMT-associated genes in MUC1-sorted MCF7 cells revealed increased vimentin expression in MUC1-High cells, and reduced E-cadherin expression in MUC1-Low cells, though the differences were not statistically significant (Fig. S5B). In comparison, integrin  $\beta 1$  levels remained relatively unaltered. Therefore, it is likely the observed mesenchymal phenotype is biophysically regulated by differential glycan expression. To check whether the cell morphology is impacted by surface glycan level, we have analyzed single-cell morphology of sorted cells grown on collagen-coated surface from phase-contrast images. While cell spread area reduced with an increase in MUC1 levels, enzymatic deglycosylation led to increase in cell spread area to levels comparable with that of MUC1-Neg cells (Fig. 4A and B). MUC1-High cells also possessed the highest circularity, which dropped to baseline levels after NMase treatment (Fig. 4A and B).

To next probe whether these observations are cell line specific or applicable to other cell types as well, we performed spreading and 2D cell motility experiments using HeLa cervical cancer cells in the presence and absence of NMase. Similar to MCF7 cells, HeLa cells were FACS sorted to obtain MUC1-Neg, MUC1-Low, and MUC1-High cells (Fig. S6A and B). While MUC1-Neg and MUC1-Low cells exhibited comparable spreading, MUC1-High HeLa cells exhibited rounded morphologies similar to MUC1-High MCF7 cells (Fig. S6C and D). As with MCF7 cells, NMase treatment abolished differences in cell spreading and circularity in HeLa cells. Motility experiments on collagen-coated dishes revealed the fastest motility in MUC1-Low cells, with NMase treatment eliminating this differential motility (Fig. S6E and F).

Alterations in cell spread area hint toward a differential regulation of cell–substrate adhesion by the cell surface glycocalyx. To

test whether cell–substrate adhesion is altered by MUC1 levels, we performed cell adhesion assay wherein MUC1-sorted MCF7 cells were allowed to adhere for 2 h on collagen-coated dishes, and then subjected to phosphate-buffered saline (PBS) wash (Fig. 4C). Nuclei-based counting revealed an inverse correlation between MUC1 levels and the proportion of attached cells, with NMase treatment leading to increased attachment of MUC1-High cells (Fig. 4C–E). In line with these observations, mucinase treatment of parental MCF7 and MDA231 cells also led to increase in cell adhesion (Fig. S4C and D). To further test how MUC1 levels influence adhesion, trypsin de-adhesion assay (28, 29) was performed, wherein spread cells were incubated with warm trypsin and their detachment kinetics tracked for the duration cells rounded up but remained attached to their substrates (Fig. 4F and G). Once again, the de-adhesion time, i.e. the time for cells to round up correlates inversely with MUC1 levels with fastest de-adhesion observed in MUC1-High cells, and NMase treatment abolishing the MUC1-dependent behavior (Fig. 4H).

Adhesion and de-adhesion experiments together suggest that glycocalyx regulates cell–substrate adhesion. To further test the molecular mechanism, we stained focal adhesions of sorted cells using paxillin staining (Fig. 5A). In comparison with small-sized focal adhesions observed in MUC1-Neg cells observed both at the cell periphery and the cell interior, prominent peripheral focal adhesions were observed in MUC1-Low cells (Fig. 5A and B). Strikingly, in MUC1-High cells, few small-sized focal adhesions were detected. This MUC1-dependent focal adhesion formation was abolished upon NMase treatment.

Phospho-focal adhesion kinase (pFAK) staining revealed the highest active focal adhesions in MUC1-Low cells compared with MUC1-Neg and MUC1-High cells, with pFAK clusters located peripherally (Fig. 5C and D). In line with the rounded morphology of MUC1-High cells, traction force microscopy (TFM) experiments revealed lowest traction exerted by these cells (Figs. 5E and S7). Traction forces increased significantly upon NMase treatment, which induced the formation of more focal adhesions. Active focal adhesion formation in MUC1-Low cells was associated with increased MMP2 localization at the cell membrane, while the total MMP2 expression remained unaltered (Fig. S8). Focal-addition dynamics of mCherry-Paxillin-transfected malignant MDA231 cells further revealed that enzymatic deglycosylation significantly reduces focal adhesion turnover rate (Fig. 5F and G). A close observation with high magnification images revealed that focal adhesion complexes are only formed at glycan excluded zones (Fig. S9), suggesting that large surface glycans sterically impede the formation of integrin-based focal adhesions, as reported earlier (20, 21). This was further highlighted by the fact that with increasing surface glycan density, cells show decreasing surface integrin (Fig. S10). Additionally, our RT-PCR experiment revealed integrin expression remained unchanged across FACS-sorted cells suggesting that MUC1 does not genetically alter integrin  $\beta 1$  expression but changes its localization (Fig. S5). Together, these experiments suggest that the surface glycocalyx regulates cell–matrix adhesions. An intermediate level of glycocalyx expression promotes integrin-based focal adhesions that are large in size and are peripherally located—a hallmark of mesenchymal cells (30–34).

## Bulky glycocalyx increases 3D invasiveness through increased cell–matrix contacts

To test how cell surface glycocalyx impacts cell migration in 3D scenario where cells are surrounded by the extracellular matrix (ECM), we have checked migration rate of MUC1-sorted cells embedded in 3D collagen hydrogels. Interestingly, both MUC1-Low

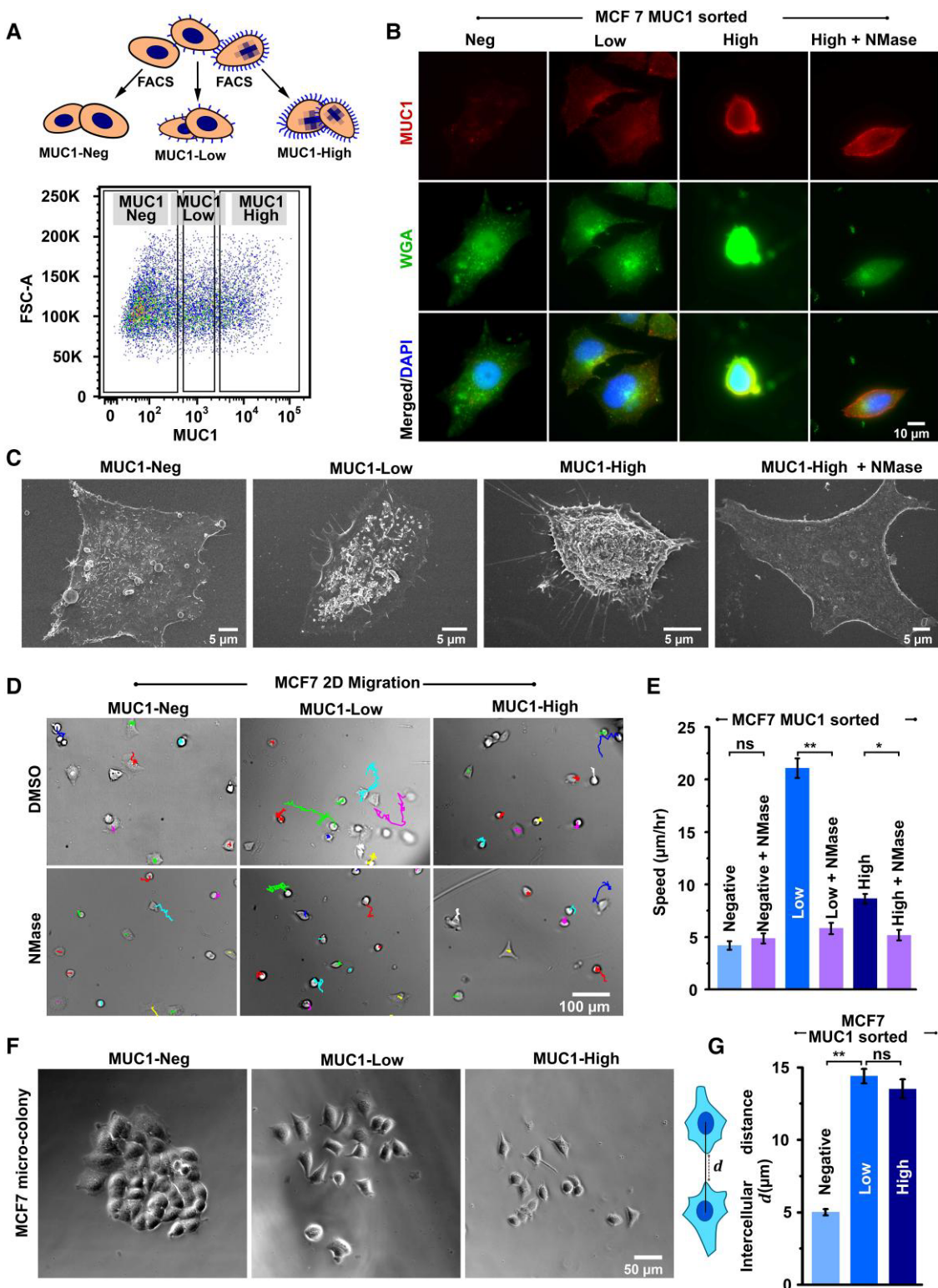


**Fig. 3.** Intermediate level of glycocalyx promotes invasiveness. A) FACS sorting of MCF7 in MUC1-Neg, intermediate (low) and high cell populations. B) MUC1 and FITC-WGA staining of FACS-sorted MC7 cells. MUC1-High-expressing cells were also de-glycosylated with NMase treatment (High + NMase). Scale bar, 10  $\mu$ m. C) FEG-SEM images showing membrane microarchitecture of FACS-sorted MCF7 cells. Scale bar, 5  $\mu$ m. D) 2D motility of FACS-sorted MCF7 cells on collagen-coated substrate with images showing representative tracts, and (E) quantification of cell speed. Scale bar, 100  $\mu$ m ( $n = 3$ , 100–150 cells per condition, ns, nonsignificant, \* $P < 0.05$ , \*\* $P < 0.005$ , data are presented as mean  $\pm$  SEM). F) Clonogenic assay showing microcolony architecture of FACS-sorted MCF7 cells. FACS-sorted cells were sparsely seeded and grown for 96 h so that cells can divide to form microcolonies. G) The graph measures the average intercellular distance between neighboring cells in each colony. Scale bar, 50  $\mu$ m ( $n = 3$ , 30–40 colonies per condition, ns, nonsignificant  $P > 0.05$ , \*\* $P < 0.005$ , data are presented as mean  $\pm$  SEM).

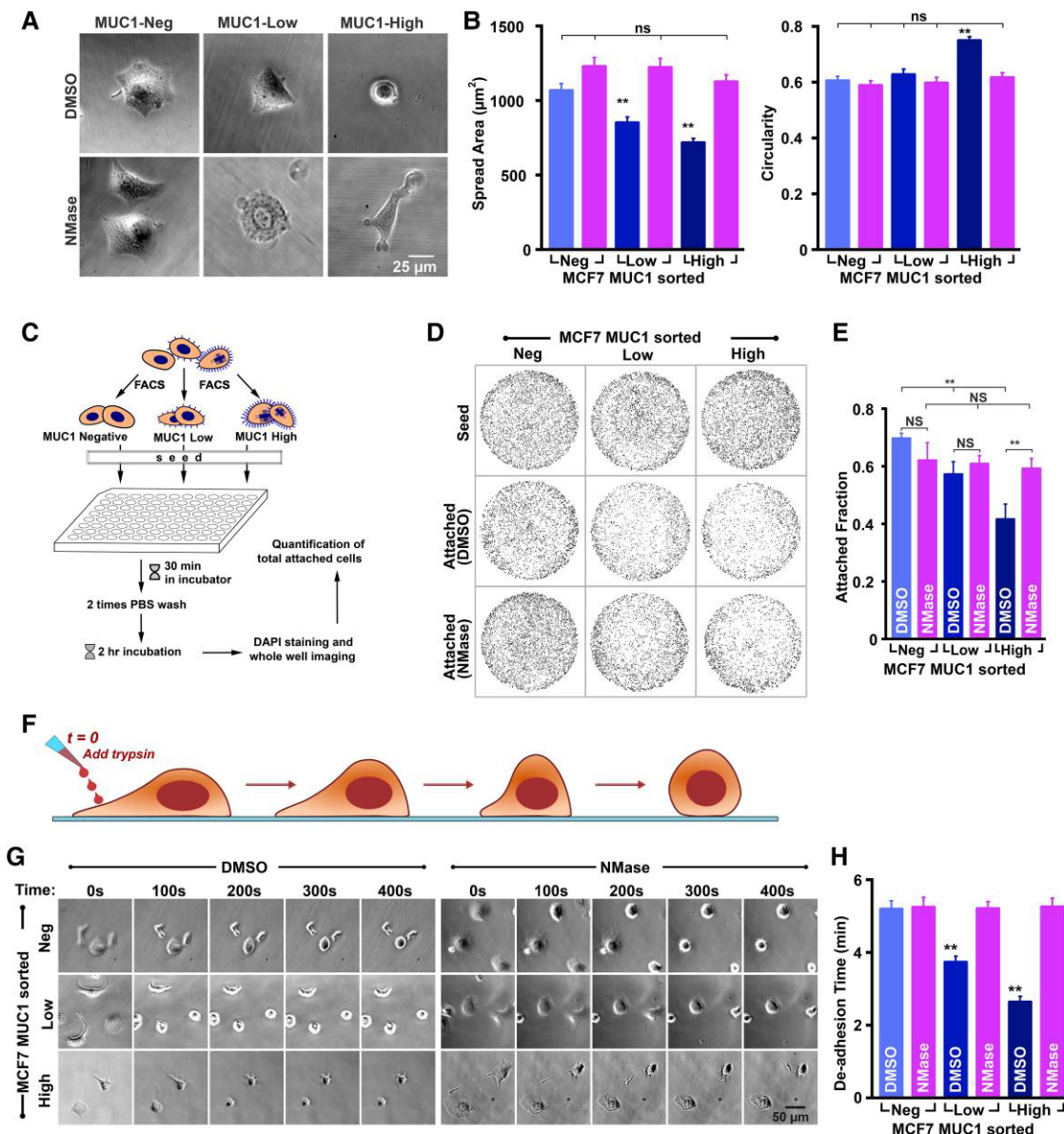


**Fig. 4.** Intermediate level of glycocalyx promotes invasiveness by regulating focal adhesions. **A)** Representative phase-contrast images showing morphology of MUC1 FACS-sorted MCF7 cells cultured on collagen-coated substrate. MCF7 cells are sorted in MUC1-Neg, intermediate (low)- and MUC1-High-expressing cell populations and were grown for 12 h in the presence of DMSO control or 0.4 U/mL NMase and 20  $\mu$ g/mL tunicamycin (NMase). **B)** Quantification of cell spread area and cell circularity from the obtained images ( $n > 100$  cells from three independent experiments, ns, nonsignificant;  $P > 0.05$ , \*\* $P < 0.005$ , data are presented as mean  $\pm$  SEM). **C)** Schematic of adhesion assay with MUC1 FACS-sorted MCF7 cells. FACS-sorted MCF7 cells were seeded in collagen-coated 96-well plate, allowed to attach for 30 min, then PBS washed, and stained with DAPI, and the whole plate was imaged using microscope to count cells. **D)** Representative images of nucleus in one well after thresholding with top row showing wells without wash step (seed) and the bottom panel showing attached cells with and without NMase treatment. **E)** Quantification of attached cell fraction (Attached fraction = Attached cells/Initial seed) ( $n = 3$ , \*\* $P < 0.005$ , ns, nonsignificant;  $P > 0.05$ , data are presented as mean  $\pm$  SEM). **F-H)** De-adhesion assay of MUC1 FACS-sorted MCF7 cells without and with enzymatic deglycosylation using NMase treatment. **F)** Schematic of the de-adhesion assay. **G)** Representative frames showing cell de-adherence over time. **H)** Graph is showing average de-adhesion time ( $n = 3$ , 90–150 cells per condition, \*\* $P < 0.005$ , Not significant (NS)  $P > 0.05$ , data are presented as mean  $\pm$  SEM).

and MUC1-High cells migrated significantly faster compared with MUC1-Neg cells, while enzymatic deglycosylation led to a near complete arrest in cell invasiveness (Fig. 6A and B). HeLa cells also showed a similar response when migrating in collagen hydrogels (Fig. S11). Cell migration often depends on how effectively cells can couple their internal actin retrograde flow with the substrate (35), which is often achieved by focal adhesions that generate traction and propel the cell forward. Cell–substrate traction can also increase by other means such as substrate typography (35). To test the hypothesis that surface glycocalyx can induce

higher cell–substrate traction through increased surface roughness, we performed scanning electron microscopy (SEM) of sorted cells and enzyme-treated cells grown on collagen-coated glass coverslips (Figs. 2B and 3C). SEM images revealed that cell surface roughness increases with increasing MUC1 level and enzymatic deglycosylation makes the cell surface smooth. Further, MCF7 MUC1-High cells produce numerous membrane protrusions that effectively increase cell surface roughness (Fig. 6C). To test how these protrusions would impact cells in 3D-ECM, we seeded cells on top of collagen hydrogel and prepared sample for SEM imaging.

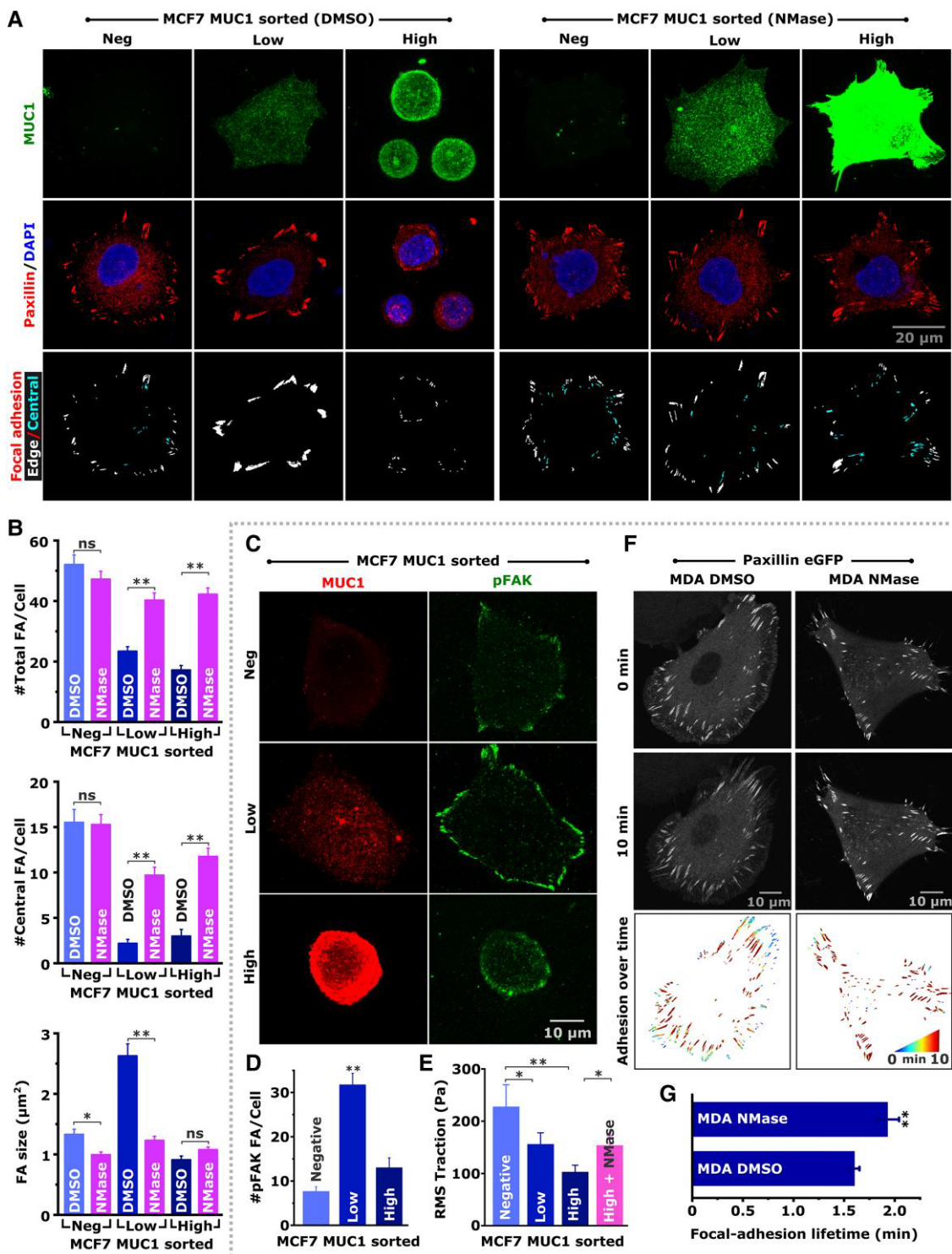


**Fig. 5.** Glycocalyx regulates focal adhesion dynamics. **A)** Representative confocal images of paxillin and MUC1 stained FACS-sorted MUC1-Neg, intermediate (low) and high MCF7 cells in the presence of DMSO control or 0.4 U/mL NMase and 20  $\mu$ g/mL tunicamycin (NMase). Nuclei stained with DAPI. Bottom panel shows focal adhesion distribution with focal adhesion at the edge in white and adhesion inside in cyan. **B)** Quantification of average number of total focal adhesion/cell, central focal adhesion/cell and average size of focal adhesions across different conditions ( $n = 3$ ,  $>50$  cells per condition,  $^{**}P < 0.005$ , ns, nonsignificant  $P > 0.05$ , data are presented as mean  $\pm$  SEM). **C)** Representative confocal images of pFAK and MUC1 stained FACS-sorted MCF7 cells. **D)** Quantification of average number of pFAK focal adhesions/cell across different conditions ( $n = 3$ , per condition  $\geq 40$  cells per condition,  $^{**}P < 0.005$ , ns,  $P > 0.05$ , data are presented as mean  $\pm$  SEM). **E)** Quantification of cell–substrate traction using TFM. Graph shows root-mean-square tractions exerted by cells grown on collagen-coated 5 kPa gels ( $^*P < 0.05$ ,  $^{**}P < 0.001$ , for  $n > 30$  cells per condition from three independent experiments, data are presented as mean  $\pm$  SEM). **F)** Focal adhesion dynamics in MDA231 cells in the presence of DMSO control or 0.4 U/mL NMase and 20  $\mu$ g/mL tunicamycin (NMase). Representative images showing focal adhesion at the beginning (0 min) and end (10 min) of experiment, and color-coded images depicting images of adhesions overlaid from multiple time points acquired over a period of 10 min. **G)** Analysis of focal adhesion lifetime ( $^*P < 0.05$ ,  $^{**}P < 0.001$ ; ns, nonsignificant  $P > 0.05$ , for  $n \geq 16$  cells analyzed per condition from three independent experiments, data are presented as mean  $\pm$  SEM).

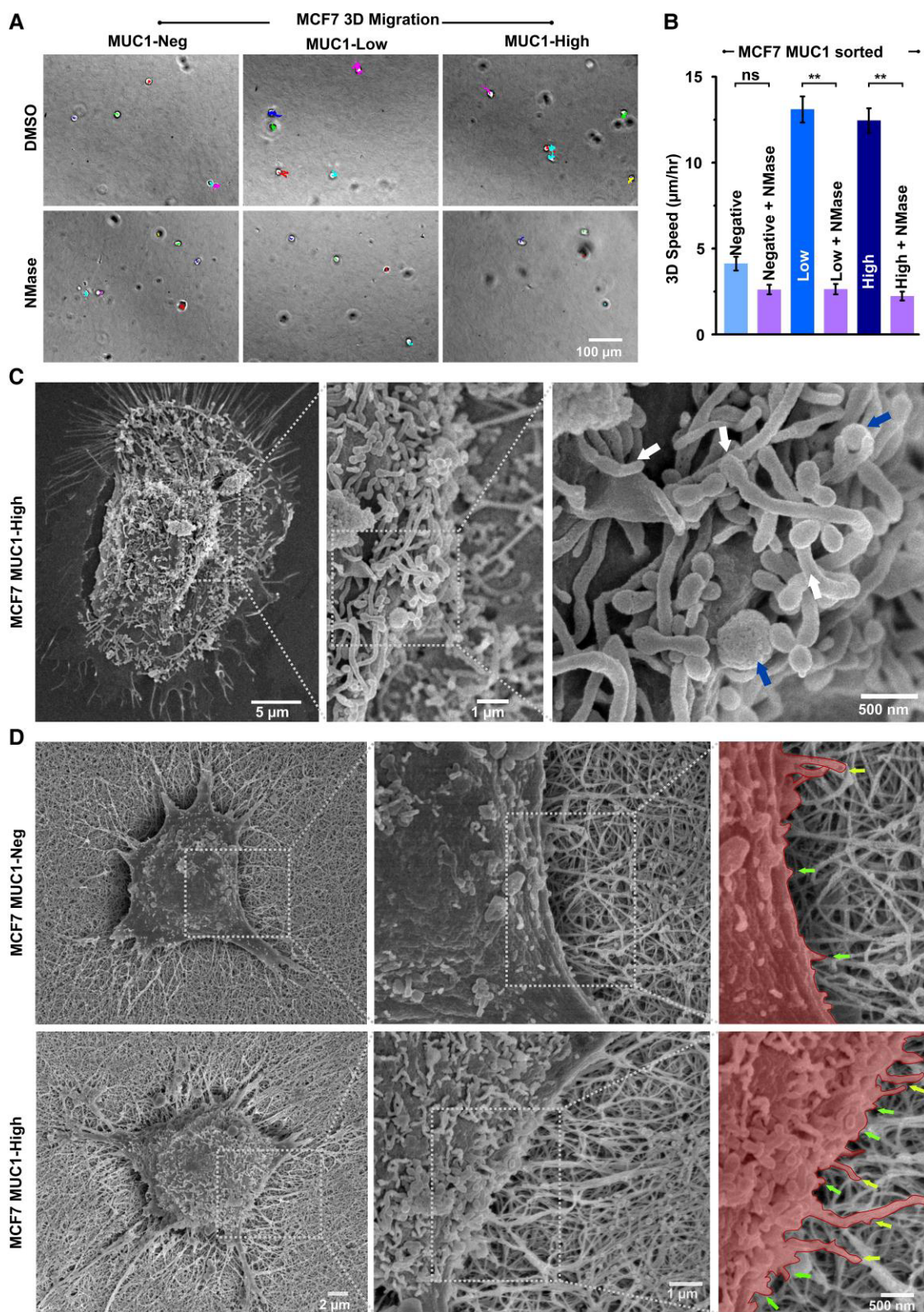


**Fig. 6.** Bulky glycocalyx increases 3D invasion by increasing cell surface traction. **A, B**) Invasiveness of MUC1-Neg, MUC1-Low, and MUC1-High MCF7 cells embedded in 3D collagen gel (1 mg/mL) with (A) showing representative microscopic frames with migration tracts and (B) quantification of cell speed. Scale bar, 100  $\mu$ m ( $n = 3$ , 65–100 cells per condition, \*\* $P < 0.005$ , data are presented as mean  $\pm$  SEM). **C**) FEG-SEM images showing membrane microarchitecture of FACS-sorted MUC1-High MCF7 cells. Cells having high glycocalyx expression exhibit numerous protrusions (white arrows) and blebs (blue arrows). **D**) FEG-SEM images of FACS-sorted MCF7 MUC1-Neg and MUC1-High cells grown on collagen hydrogels. Right panel shows magnified inset with cell pseudo-colored in red shows more membrane micro-ridge (green arrows) and protrusions (yellow arrow) tangled in collagen hydrogels that likely increases membrane traction.

SEM images revealed that the cell–substrate interface of high mucin-expressing cells is rougher with numerous protrusions entangled in the collagen network (Fig. 6D). Such entanglements with the ECM may serve as transient adhesions that propel the cell forward during 3D migration.

### Bulky glycocalyx confers shear resistance and increased E-selectin adhesion

Low adhesion and circular morphology of MUC1-High cells show striking similarities with circulating tumor cells (CTCs) that are often found in the vasculature. To test whether high levels of MUC1 can facilitate vascular metastasis, we have done experiments with 200 ng/mL E-selectin-coated substrates as E-selectin coating mimics the vascular endothelial lining (36–38). While cell spread area decreases with increasing MUC1 level on collagen-coated substrates (Fig. 4A and B), cells exhibit the opposite response on E-selectin-coated surfaces, i.e. with increasing MUC1 levels, cell adhesion increases on E-selectin-coated substrates (Fig. S12A and B). This suggests that the glycocalyx regulates adhesion in a substrate-dependent manner. To test this further, we performed adhesion experiments on E-selectin-coated plates with MUC1-sorted cells. This experiment also revealed increased attachment with increasing MUC1 levels, and NMase treatment abolished this dependence (Fig. S12C and D). While spreading was MUC1-dependent, cell motility on selectin-coated surfaces was insensitive to MUC1 levels (Fig. S12E and F).

To probe the nature of selectin adhesions, cells cultured on selectin and collagen-coated substrates were stained for paxillin and MUC1. In contrast to collagen-coated substrates where prominent paxillin-positive focal adhesions were detected, both the number and size of focal adhesions were dramatically reduced on 200 ng/mL selectin-coated substrates (Fig. S13A–C). On substrates coated with 10 ng/mL selectin (i.e. 20-fold dilution), an increase in the number and size of focal adhesions was observed. Moreover, we noticed the presence of small MUC1 puncta reminiscent of adhesion complexes alongside focal adhesions (Fig. S13D). Collectively, these results suggest MUC1 mediates adhesion formation of selectin-coated substrates, with increased MUC1-selectin adhesions leading to reduced formation of focal adhesions. Thus, the insensitivity of cell motility to MUC1 levels may be attributed to the formation of a minimal number of focal adhesions.

E-selectin coating alone does not fully recapitulate the vascular system in the absence of vascular fluid flow. To simulate the vascular system, we seeded cells on E-selectin-coated channel (microfluidic device) connected to a syringe pump that can generate fluid (media) flow inside the channel. Live imaging at increasing flow rates revealed that with an increase in MUC1 expression, cells take longer to detach, while MUC1-Neg exhibited fastest detachment (Fig. 7A and B, Movie S1). Detachment of MUC1-High cells—which exhibited the strongest resistance to shear stresses—was significantly hastened upon enzymatic deglycosylation. WGA-stained live imaging at high magnification revealed that cells shed glycocalyx and leave a trail of glycocalyx attached to the substrate (Fig. S14A and Movie S2). Cells are also known to regenerate the surface glycocalyx (39, 40) (Fig. S14B and C). Collectively, these results are indicative of a protective role of the surface glycocalyx during migration in the vasculature. While E-selectin–glycan adhesions are broken by glycocalyx shedding when the cell is subjected to excessive flow-induced shear stress, these adhesions can be later replenished via glycocalyx regeneration (41–43).

Based on our in vitro data, we hypothesized that the expression of MUC1 in CTCs would be more heterogeneous compared with primary tumor cells. To understand the MUC1 expression in patient samples, we analyzed single-cell RNA-sequencing data of patient CTCs and primary tumors of breast cancer. In support of our hypothesis, we observed that CTCs exhibit greater heterogeneity in MUC1 expression than primary tumor cells, as quantified by measuring the coefficient of variation, CV = 1.55 for CTCs and 1.09 for primary tumors (Fig. S15). This enhanced heterogeneity in MUC1 expression in CTCs may contribute to their survival and resistance to the mechanical stresses encountered in the bloodstream.

## Discussion

Glycocalyx composition and organization change significantly with the cancer progression. Overexpression of several glycocalyx-associated proteins, including MUC1 has been reported in multiple cancers, including breast cancer, lung cancer, pancreatic cancer, ovarian cancer, prostate, and bladder cancer (6, 13, 44–47). While MUC1 has long been known to be associated with malignancy (12, 13), most of the mucin research has been focused on its cytosolic domain which participates in various cancer-associated signaling cascades. The presence of bulky glycocalyx at the cancer cell surface is a rather recent finding (7).

In this study, we demonstrate that a bulky glycocalyx—by being an effective spacer between cell membrane and the substrate—can physically regulate cell–substrate adhesion dynamics and integrin signaling. Then, it acts as a cell adhesion molecule that selectively binds to selectins that are abundantly present in endothelial cells lining blood vessels and thus helps in vascular migration (36, 48, 49). Additionally, the glycocalyx can contribute significantly to cell membrane shape regulation and help in membrane protrusion formation. The increased membrane microprotrusions can increase membrane roughness and increase cell–substrate traction forces leading to increased cell migration. Since the glycocalyx facilitates membrane protrusion and eases membrane bending, this would likely ease the formation of protrusive structures such as filopodia and lamellipodia.

Our initial experiments revealed that cell surfaces of MCF7, MDA231 breast cancer cells, and HeLa cervical cancer cells are decorated with MUC1. Both MCF7 and MDA231 cells are overall more glycocalyx enriched compared with nonmalignant MCF10A cells. This higher expression of bulky glycocalyx increases cell migration and invasion, which decreases upon enzymatic deglycosylation.

Cells exhibit diffused adhesions in the absence of a glycocalyx as bulky glycocalyx prevents adhesion formation by expanding the gap between the cell membrane and the ECM (19–21). Cells in the presence of excess bulky glycocalyx, therefore, form integrin clusters at glycan excluded zones that forms clustered focal adhesions. Based on this, we hypothesized that optimal surface glycan levels enhance cell migration rate by optimally regulating cell–ECM adhesion, with the absence of glycocalyx hindering cell migration through increased adhesion formation, and excess glycocalyx preventing integrin-based adhesions altogether. Our experiments with FACS-sorted MCF7 and HeLa cells indeed confirmed that cells expressing intermediate MUC1 levels migrate faster than mucin-negative and MUC1-High-expressing cells. Further investigation revealed this high cell migration speed is indeed caused by an optimal adhesion–deadhesion rate. Cells expressing an intermediate level of mucin have fewer focal adhesion and optimal focal adhesion turnover compare with

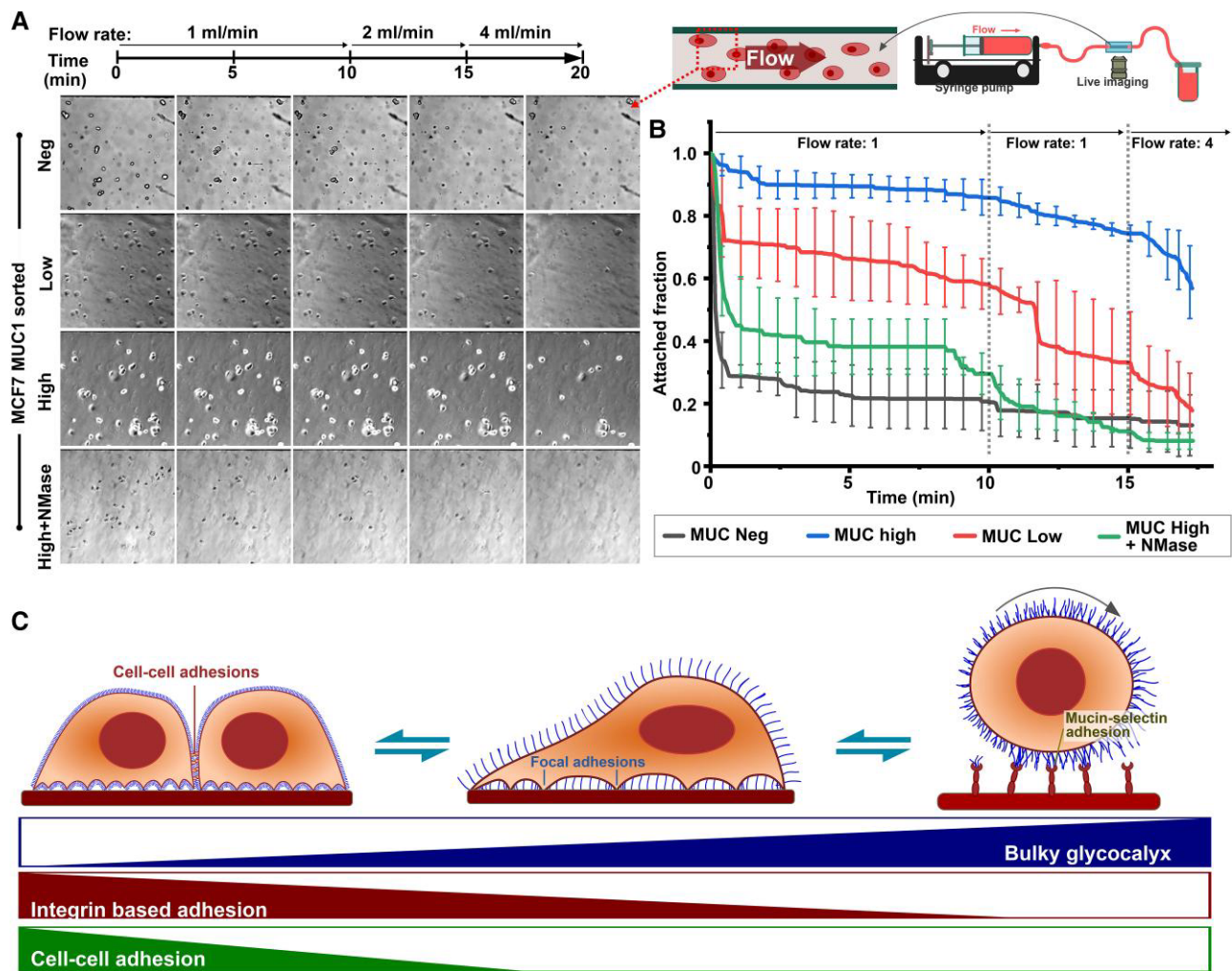


**Fig. 7.** Bulky glycocalyx confers shear resistance. A) FACS-sorted MCF7 cells seeded inside selectin-coated microfluidics channels were subjected to different flow-induced shear stresses and imaged using a live-cell imaging setup. Representative phase-contrast images showing a section of the channel at different time points with attached cells. B) Quantification of remaining attached cell fraction across different conditions, as they are subjected to flow-induced shear stress ( $n \geq 3$ , data are presented as mean  $\pm$  SEM). C) Schematic showing bulky glycocalyx-mediated cancer progression. Cells form diffused cell-substrate adhesion and retain intact cell-cell adhesion at low bulky glycocalyx level resembling an epithelial phenotype. As bulky glycocalyx increases to an intermediate level, these cells transit to a mesenchymal phenotype, where the cell loses cell-cell adhesion and gains clustered focal adhesion largely driven by glycocalyx-induced repulsion. Further glycocalyx upregulation causes a complete loss of integrin-based adhesion and induces a phenotype similar to CTCs. A high level of surface glycocalyx may mediate selectin-based adhesion inside blood vessel and help in intravascular metastasis.

mucin-negative cells which contribute to a faster migration. High mucin-expressing cells are unable to form a sufficient adhesion to sustain adhesion-dependent migration.

Circulating tumor cells are known to further up-regulate surface glycocalyx. It has been shown to have the highest level of glycocalyx expression. The cell surface glycocalyx can act as receptor molecules that can bind to selectins present on the surface of the vascular endothelial cells. Thus, the glycocalyx acts as adhesion molecules when the cancer cells are migrating through the blood vessels as circulating tumor cells. This is evident from the fact that MUC1-High-expressing cells attach more strongly and spread more on selectin-coated substrates compared with MUC1-Low-expressing cells. Additionally, on selectin-coated microfluidic channels, MUC1-High-expressing MCF7 cells were found to resist vascular fluid flow to the greatest extent and stay attached to the substrate. Further, the cells might follow a rolling mode of migration, which are often seen with leucocyte cells migrating through blood vessels (50, 51).

Based on our findings, we propose a mode of cancer metastasis dominated by surface glycocalyx expression: cells exhibit diffused adhesion with intact cell-cell adhesions at low bulky glycocalyx level resembling epithelial cells. With increasing glycocalyx, at intermediate levels, these cells transit to a mesenchymal-like state, where cells lose cell-cell adhesions and gain clustered focal adhesions. Further upregulation causes the cells to lose integrin-based adhesions altogether and prepares them for intravascular metastasis as CTCs that are largely mediated by E-selectin-glycan adhesion (Fig. 7C).

Apart from regulating cell-matrix adhesions, glycocalyx has also been shown to regulate cell membrane microarchitecture (22, 52). Our SEM imaging experiments revealed the presence of micro-protrusions and small membrane blebs on the cell surface which disappear upon enzymatic deglycosylation. Furthermore, lack of these structures in MUC1-Neg cells suggests that a bulky glycocalyx drives the formation of these membrane structures. Glycocalyx helps the formation of these micro-protrusions by

decreasing membrane bending energy (22, 23). Glycan-contributed membrane micro-protrusions lead to increased membrane roughness and generate membrane tractions that enable faster cell migration, as observed in our experiments (Figs. 3C and 6). These structures would additionally stabilize larger membrane protrusion in the 3D-ECM network by tangling with the fibrous network and forming integrin independent adhesions (Fig. 6D).

Overall, our study provides interesting insights into the biophysical role of cell surface glycocalyx in cancer cell invasion, adhesion regulation, and regulation of cell membrane biophysics.

## Materials and methods

Detailed materials and methods are provided in the supplementary section as extended materials and methods.

## Cell lines and experiment conditions

MCF7, HeLa, and MDA231 cell lines obtained from the National Center for Cell Science, Pune, India, were cultured according to standard protocol. About 10 µg/cm<sup>2</sup> collagen type I (Sigma, Cat #C3867)- or 0.2 µg/mL E-selectin (Cat #724-ES, R&D Systems)-coated substrates were used for experiments. Cells were treated with NMase (Sigma, Cat #N2876) to remove surface glycocalyx and tunicamycin (Sigma, Cat #T7765) was used to prevent new glycosylation (27, 53). About 500 mU/mL NMase containing 20 µg/mL tunicamycin was used for all the experiments based on viability assessment by MTT assay (Fig. S2). Cells were treated with the enzyme cocktail for 2 h prior to all experiments.

FACS sorting: Trypsinized cells stained with Fluorescein isothiocyanate (FITC)-conjugated antihuman MUC1 antibody (BD, Cat #559774) were analyzed or sorted in sterile FACS tubes for further experiments using a BD FACS Aria III Cell Sorter.

## Single-cell biophysical measurements

Motility videos were obtained from sparsely seeded cells (2,000 cells/cm<sup>2</sup>) on collagen or selectin-coated 48-well or cells embedded in 3D collagen (Corning, Ref #354249) using an Olympus inverted microscope (Olympus IX83). Cell trajectories and speed were measured from obtained videos using the manual track plugin in Fiji-ImageJ. Cell spheroids generated by hanging drop method (54) embedded in 3D collagen gels were imaged every 24 h and its spread area was calculated and compared with the initial spheroid size from the acquired images. Six- to 8-day-old microcolony from sparsely seeded cells was imaged, and colony features like cell–cell distance were measured using ImageJ.

Experimental cells were seeded on Collagen or E-selectin-coated 96-well plates for 30 min at 37 °C. After gentle washing with warm PBS, attached cells were fixed and stained with DAPI to visualize the nuclei. Entire wells were then imaged using and the number of attached cells/well was counted from the obtained images using ImageJ. De-adhesion assay was performed using protocol described elsewhere (29, 55) after growing cells on collagen/E-selectin-coated dishes for 24 h. mCherry-Paxillin-transfected cells were used for focal adhesion dynamics (56). Focal adhesion lifetime was analyzed from acquired using protocols, as described elsewhere (57).

A straight 400 µm microfluidic channel coupled to a syringe pump was used for shear experiments (Fig. 7A). The experiment procedure is detailed in the [Supplementary material](#).

## Microscopy

Imaging techniques and sample preparation protocol are detailed in the [Supplementary material](#). Fixed and immunostained samples were imaged using a scanning probe confocal microscope (LSM 780, Zeiss) using 63x objective and electron microscopy samples were imaged using Joel JSM-7600F scanning electron microscope. Images were processed and analyzed using Fiji-ImageJ software.

## Immunohistochemistry, cCNA, and RNA-sequencing analysis

Details of the immunohistochemistry of patient samples and scoring methods on formalin-fixed paraffin-embedded tissue are also included in the [Supplementary Methods](#). CNA analysis using cBioPortal (58), single-cell RNA-sequencing data analysis from the GEO accession number GSE109761 (59), and details of EMT score calculation are described in detail in the [Supplementary Methods](#). The PCR data were analyzed using comparative Ct method, which is explained in detail in the [Supplementary Methods](#).

## Statistical analysis

The data distribution was tested using the Kolmogorov–Smirnov normality test. Based on the outcome, either a parametric or a nonparametric statistical test was performed. For parametric data, statistical analysis was performed using one-way ANOVA and Fisher's test was used to compare the means. Mann–Whitney test was performed for nonparametric data. Statistical analysis was performed using Origin 9.1 (OriginLab Corporation), with  $P < 0.05$  considered to be statistically significant.

## Acknowledgments

Authors acknowledge IIT Bombay for providing Flow Cytometry (FACS) facility, Cryo Field emission scanning electron microscopy (FEG-SEM) and Confocal Microscopy facilities.

## Supplementary Material

[Supplementary material](#) is available at PNAS Nexus online.

## Funding

S.S. acknowledges funding support from the Department of Science and Technology, Ministry of Science and Technology (DST/SJF/LSA-01/2016-17), Science and Engineering Research Board, Government of India (CRG/2022/001218), M.K. acknowledges the DBT-Ramalingaswami “re-entry” fellowship and the DBT-Basic Research in Biology awarded by DBT-India and a research grant to CTCR by Bajaj Auto Ltd.

## Author Contributions

A.B. and S.S. conceived the study and wrote the manuscript. A.B., N.P., S.K.S., and S.D. performed the cell experiments. V.G. and M.K. helped with the IHC. M.M.G. and S.K. helped with the *in silico* analysis.

## Preprints

This manuscript was posted on a preprint: DOI: 10.1101/2023.08.03.551677.

## Data Availability

All data needed to evaluate the conclusions in the paper are present in the paper and/or the [Supplementary Material](#).

## References

- 1 Khalili AA, Ahmad MR. 2015. A review of cell adhesion studies for biomedical and biological applications. *Int J Mol Sci.* 16: 18149–18184.
- 2 Burridge K, Fath K, Kelly T, Nuckolls G, Turner C. 1988. Transmembrane junctions between the extracellular matrix and the cytoskeleton. *Annu Rev Cell Biol.* 4:487–525.
- 3 Kanchanawong P, Calderwood DA. 2023. Organization, dynamics and mechanoregulation of integrin-mediated cell–ECM adhesions. *Nat Rev Mol Cell Biol.* 24:142–161.
- 4 Kechagia JZ, Ivaska J, Roca-Cusachs P. 2019. Integrins as biomechanical sensors of the microenvironment. *Nat Rev Mol Cell Biol.* 20:457–473.
- 5 Martínez-Palomo A. 1970. The surface coats of animal cells. *Int Rev Cytol.* 29:29–75.
- 6 Lakshmanan I, et al. 2015. Mucins in lung cancer: diagnostic, prognostic, and therapeutic implications. *J Thorac Oncol.* 10: 19–27.
- 7 Iyer S, Gaikwad RM, Subba-Rao V, Woodworth CD, Sokolov I. 2009. Atomic force microscopy detects differences in the surface brush of normal and cancerous cells. *Nat Nanotechnol.* 4:389–393.
- 8 Dokukin M, et al. 2016. Pericellular brush and mechanics of Guinea pig fibroblast cells studied with AFM. *Biophys J.* 111: 236–246.
- 9 Higashi M, et al. 1999. Expression of MUC1 and MUC2 mucin antigens in intrahepatic bile duct tumors: its relationship with a new morphological classification of cholangiocarcinoma. *Hepatology.* 30:1347–1355.
- 10 Nath S, Mukherjee P. 2014. MUC1: a multifaceted oncoprotein with a key role in cancer progression. *Trends Mol Med.* 20:332–342.
- 11 Brockhausen I. 2006. Mucin-type O-glycans in human colon and breast cancer: glycodynamics and functions. *EMBO Rep.* 7: 599–604.
- 12 Imai K, et al. 2001. MUC1 as a human tumor marker. *Int Congr Ser.* 1223:125–133.
- 13 Taylor-Papadimitriou J, Burchell J, Miles DW, Dalziel M. 1999. MUC1 and cancer. *Biochim Biophys Acta.* 1455:301–313.
- 14 Satoh S, et al. 2000. Enhancement of metastatic properties of pancreatic cancer cells by MUC1 gene encoding an anti-adhesion molecule. *Int J Cancer.* 88:507–518.
- 15 Suwa T, et al. 1998. Increased invasiveness of MUC1 cDNA-transfected human gastric cancer MKN74 cells. *Int J Cancer.* 76: 377–382.
- 16 Jeong SJ, et al. 2018. Inhibition of MUC1 biosynthesis via threonyl-tRNA synthetase suppresses pancreatic cancer cell migration. *Exp Mol Med.* 50:e424.
- 17 Xu HL, Zhao X, Zhang KM, Tang W, Kokudo N. 2014. Inhibition of KL-6/MUC1 glycosylation limits aggressive progression of pancreatic cancer. *World J Gastroenterol.* 20:12171–12181.
- 18 Besmer DM, et al. 2011. Pancreatic ductal adenocarcinoma (PDA) mice lacking mucin 1 have a profound defect in tumor growth and metastasis. *Cancer Res.* 71:4432–4442.
- 19 Ewald AJ, Egeblad M. 2014. Cancer: sugar-coated cell signalling. *Nature.* 511:298–299.
- 20 Paszek MJ, Boettiger D, Weaver VM, Hammer DA. 2009. Integrin clustering is driven by mechanical resistance from the glycocalyx and the substrate. *PLoS Comput Biol.* 5:1000604.
- 21 Paszek MJ, et al. 2014. The cancer glycocalyx mechanically primes integrin-mediated growth and survival. *Nature.* 511: 319–325.
- 22 Carolyn Shurer AR, et al. 2019. Physical principles of membrane shape regulation by the glycocalyx correspondence. *Cell.* 177: 1757–1770.e21.
- 23 Kuo JCH, Paszek MJ. 2021. Glycocalyx curving the membrane: forces emerging from the cell exterior. *Annu Rev Cell Dev Biol.* 37:257–283.
- 24 Kufe DW. 2009. Mucins in cancer: function, prognosis and therapy. *Nat Rev Cancer.* 9:874–885.
- 25 Horm TM, Schroeder JA. 2013. MUC1 and metastatic cancer expression. Function and therapeutic targeting. *Cell Adh Migr.* 7:187–198.
- 26 Ho JJL, Cheng S, Kim YS. 1995. Access to peptide regions of a surface mucin (MUC1) is reduced by sialic acids. *Biochem Biophys Res Commun.* 210:866–873.
- 27 Crean SM, et al. 2004. N-linked sialylated sugar receptors support haematopoietic cell-osteoblast adhesions. *Br J Haematol.* 124: 534–546.
- 28 Sen S, Kumar S. 2009. Cell-matrix de-adhesion dynamics reflect contractile mechanics. *Cell Mol Bioeng.* 2:218–230.
- 29 Soumya SS, Sthanam LK, Padinhateeri R, Inamdar MM, Sen S. 2014. Probing cellular mechanoadaptation using cell-substrate de-adhesion dynamics: experiments and model. *PLoS One.* 9: e106915.
- 30 Levental KR, et al. 2009. Matrix crosslinking forces tumor progression by enhancing integrin signaling. *Cell.* 139:891–906.
- 31 Leggett SE, Hruska AM, Guo M, Wong IY. 2021. The epithelial-mesenchymal transition and the cytoskeleton in bioengineered systems. *Cell Commun Signal.* 19:32.
- 32 Huang RYJ, Guilford P, Thiery JP. 2012. Early events in cell adhesion and polarity during epithelial-mesenchymal transition. *J Cell Sci.* 125:4417–4422.
- 33 Nagano M, Hoshino D, Koshikawa N, Akizawa T, Seiki M. 2012. Turnover of focal adhesions and cancer cell migration. *Int J Cell Biol.* 2012:310616.
- 34 Pawlak G, Helfman DM. 2001. Cytoskeletal changes in cell transformation and tumorigenesis. *Curr Opin Genet Dev.* 11:41–47.
- 35 Lämmermann T, et al. 2008. Rapid leukocyte migration by integrin-independent flowing and squeezing. *Nature.* 453:51–55.
- 36 Mitchell MJ, King MR. 2014. Physical biology in cancer. 3. The role of cell glycocalyx in vascular transport of circulating tumor cells. *Am J Physiol Cell Physiol.* 306:C89–C97.
- 37 Smadja DM, Mulliken JB, Bischoff J. 2012. E-selectin mediates stem cell adhesion and formation of blood vessels in a murine model of infantile hemangioma. *Am J Pathol.* 181:2239–2247.
- 38 Silva M, Videira PA, Sackstein R. 2018. E-selectin ligands in the human mononuclear phagocyte system: implications for infection, inflammation, and immunotherapy. *Front Immunol.* 8:1878.
- 39 Kufe DW. 2009. Functional targeting of the MUC1 oncogene in human cancers. *Cancer Biol Ther.* 8:1197–1203.
- 40 Julian JA, Carson DD. 2002. Formation of MUC1 metabolic complex is conserved in tumor-derived and normal epithelial cells. *Biochem Biophys Res Commun.* 293:1183–1190.
- 41 McDermott KM, et al. 2001. Overexpression of MUC1 reconfigures the binding properties of tumor cells. *Int J Cancer.* 94:783–791.
- 42 Fernandez-Rodriguez J, Dwir O, Alon R, Hansson GC. 2001. Tumor cell MUC1 and CD43 are glycosylated differently with Sialyl-Lewis a and x epitopes and show variable interactions with E-selectin under physiological flow conditions. *Glycoconj J.* 18:925–930.

- 43 Geng Y, Yeh K, Takatani T, King MR. 2012. Three to tango: MUC1 as a ligand for both E-selectin and ICAM-1 in the breast cancer metastatic cascade. *Front Oncol.* 2:76.
- 44 Ajioka Y, Allison LJ, Jass JR. 1996. Significance of MUC1 and MUC2 mucin expression in colorectal cancer. *J Clin Pathol.* 49:560–564.
- 45 Burdick MD, Harris A, Reid CJ, Iwamura T, Hollingsworth MA. 1997. Oligosaccharides expressed on MUC1 produced by pancreatic and colon tumor cell lines. *J Biol Chem.* 272:24198–24202.
- 46 Girling A, et al. 1989. A core protein epitope of the polymorphic epithelial mucin detected by the monoclonal antibody SM-3 is selectively exposed in a range of primary carcinomas. *Int J Cancer.* 43:1072–1076.
- 47 Rachagani S, Torres MP, Moniaux N, Batra SK. 2009. Current status of mucins in the diagnosis and therapy of cancer. *BioFactors.* 35:509–527.
- 48 Bendas G, Borsig L. 2012. Cancer cell adhesion and metastasis: selectins, integrins, and the inhibitory potential of heparins. *Int J Cell Biol.* 2012:676731.
- 49 Hollingsworth MA, Swanson BJ. 2004. Mucins in cancer: protection and control of the cell surface. *Nat Rev Cancer.* 41:45–60.
- 50 Rejniak KA. 2016. Circulating tumor cells: when a solid tumor meets a fluid microenvironment. *Adv Exp Med Biol.* 936:93–106.
- 51 Norman KE, Moore KL, McEver RP, Ley K. 1995. Leukocyte rolling in vivo is mediated by P-selectin glycoprotein ligand-1. *Blood.* 86: 4417–4421.
- 52 Bennett RJ, et al. 2001. Mucin MUC1 is seen in cell surface protrusions together with ezrin in immunoelectron tomography and is concentrated at tips of filopodial protrusions in MCF-7 breast carcinoma cells. *J Histochem Cytochem.* 49:67–77.
- 53 Lillehoj EP, et al. 2019. Neuraminidase 1-mediated desialylation of the mucin 1 ectodomain releases a decoy receptor that protects against *Pseudomonas aeruginosa* lung infection. *J Biol Chem.* 294:662.
- 54 Foyt R. 2011. A simple hanging drop cell culture protocol for generation of 3D spheroids. *J Vis Exp.* 51:2720.
- 55 Sen S, Ng WP, Kumar S. 2011. Contractility dominates adhesive ligand density in regulating cellular de-adhesion and retraction kinetics. *Ann Biomed Eng.* 39:1163–1173.
- 56 Barai A, Mukherjee A, Das A, Saxena N, Sen S. 2021.  $\alpha$ -Actinin-4 drives invasiveness by regulating myosin IIB expression and myosin IIA localization. *J Cell Sci.* 134:jcs258581.
- 57 Berginski ME, Gomez SM. 2013. The focal adhesion analysis server: a web tool for analyzing focal adhesion dynamics. *F1000Res.* 2:68.
- 58 Cerami E, et al. 2012. The cBio cancer genomics portal: an open platform for exploring multidimensional cancer genomics data. *Cancer Discov.* 2:401–404.
- 59 Szczerba BM, et al. 2019. Neutrophils escort circulating tumour cells to enable cell cycle progression. *Nature.* 566:553–557.